PHYSICAL REVIEW A VOLUME 27, NUMBER 6 JUNE 1983

High-resolution studies on bound odd-parity Rydberg states in Ba I

E. R. Eliel* and W. Hogervorst
Natuurkundig Laboratorium der Vrije Universiteit, De Boelelaan 1081, 1081-HV Amsterdam, The Netherlands
(Received 22 November 1982)

A study of the detailed structure of the bound odd-parity Rydberg states of barium has been undertaken using a cw dye laser in combination with an atomic beam. Special attention has been paid to the $6snf$ configurations, of which the hyperfine structure has been analyzed in terms of a small set of parameters. In addition to an effective Slater-exchange integral, an effective spin-orbit interaction, and a contact hyperfine parameter, a new parameter representing two-body magnetic effects, has been introduced. The introduction of this new parameter is discussed in some detail. Good agreement between the calculated and experimental hyperfine energies is achieved in this way.

I. INTRODUCTION

The recent application of narrow-band cw dye lasers to the study of the detailed structure of the spectra of the alkaline-earth elements has considerably extended our understanding of these atoms. In the bound Rydberg states of the atoms with two valence electrons one electron is excited to a weakly bound orbit while the quantum state of the other electron is essentially unchanged. Atomic parameters, which depend on the state of excitation of the outer electron or on the interaction of the two electrons are expected to vary smoothly as a function of the effective principal quantum number n^*.

Configurations where both electrons are excited can interact with Rydberg series of the same parity. The various fine-structure states of these doubly excited configurations, dispersed over a relatively wide range of energy, each interact in a relatively small energy interval with bound Rydberg states. The wave function of such a doubly excited state is generally quite different from the wave function of the unperturbed Rydberg configurations. Consequently, their presence can induce drastic irregularities in properties such as radiative lifetime or polarizability when the whole Rydberg series is considered. For this reason these levels are generally referred to as perturbers and the Rydberg series is called perturbed. A major motive for the interest in the detailed structure of Rydberg states of these two-electron systems, is the possibility of extracting quantitative information on configuration interaction using such atomic properties as sensitive probes.

Although a wealth of data has been acquired on various properties of Rydberg states of the heavier alkaline-earth elements Ca, Sr, and Ba, most of the results pertain to perturbed series and relatively little is known on the detailed structure of unperturbed Rydberg series.

A first effort at unraveling detailed structure in configurations of essentially unperturbed series has been undertaken by Barbier and Champeau,[1] who probed the structure of $6snd$ Rydberg configurations in ytterbium, which in many aspects can be considered a two-electron atom. However, due to their limited signal to noise and resolving power only the strongest spectral components were observed, precluding a detailed analysis. Nevertheless it was concluded that the structure of essentially all Rydberg configurations can be explained in terms of simple atomic theory. These results clearly showed the relevance of applying cw dye lasers to the study of these highly excited states in order to test the applicability of simple atomic theory more rigorously.

The effort to investigate various properties of Rydberg states of the alkaline-earth elements is almost exclusively directed at the even-parity levels, as a consequence of technological limitations. The even-parity levels with $J \leq 2$ can be populated by either a two-photon or a two-step excitation process from the $^1S_0$ ground states. With available cw dye lasers only a three-step excitation process from the ground state leads to the odd-parity levels.

In barium however, the $6snp$ and $6snf$ Rydberg configurations can be studied with a frequency-doubled cw dye laser using a single-photon absorption process starting from the various fine-structure levels of the metastable $5d\,6s$ configuration. In this paper we present the results of these experiments.

The $6snp$ levels were studied previously by Garton

and Tomkins in a classical absorption experiment ($6s^2\,{}^1S_0 \rightarrow 6snp\,{}^1P_1$).[2] In addition to the level energies of the Rydberg states up to $n=75$ valuable information on the autoionizing states with orbital angular momentum $l=1$ was obtained.

Armstrong *et al.* expanded the study of bound $l=1$ states to the $^3P_1$ and $^3P_2$ levels in a three-step excitation scheme employing pulsed tunable dye lasers.[3] The $J=0$ members of the $6snp$ configurations escaped detection.

In the experiment of Armstrong *et al.* a number of $6snf$ states ($9 \leq n \leq 25$) and $6sng$ levels ($12 \leq n \leq 68$) were excited as well, the latter due to single-photon absorption from the collisionally populated $5d\,6p\,{}^1F_3$.[4] Together with the experimental data on the $6snp$ states Armstrong *et al.* presented a detailed multichannel quantum-defect theory (MQDT) analysis of the odd-parity $J=1$ series with eight interacting channels. In addition to predicting the bound-state energies to within 0.03 cm^{-1} of the observed value, the "Fano minimum" in the oscillator strength $6s^2\,{}^1S_0 \rightarrow 6snp\,{}^1P_1$, which had been observed earlier by Garton and Tomkins, is reproduced in this analysis. The energy level structure of the $J=1$ states indicate that the $6snp\,{}^3P_1$ states behave quite differently from the $6snp\,{}^1P_1$ states, although they are both included in a single MQDT analysis. In contradistinction to the $^1P_1$ states the $^3P_1$ states are unperturbed for $n>20$. The odd-parity $J=2$ states have also been analyzed in the framework of MQDT requiring a two-channel treatment only.[3]

The $6snf$ levels have been observed in a classical absorption experiment by Carlsten *et al.* starting from the metastable $5d\,6d\,{}^3D$ multiplet, populated by laser-assisted optical pumping via the $6snp\,{}^3P_1$ state.[4] The line series ${}^3D_1 \rightarrow 6snf\,{}^3F_2$, ${}^3D_2 \rightarrow 6snf\,{}^3F_3$, and ${}^3D_3 \rightarrow 6snf\,{}^3F_4$ were observed between $n=4$ and $n \sim 30$. The $6snf$ $J=2$, 3, and 4 series are generally considerd to be unperturbed (Camus *et al.*[5]) or very weakly perturbed at $n=20$ (Armstrong *et al.*).

In the present paper the results of high resolution laser-spectroscopic studies are presented with particular emphasis on the $6snf$ configurations. The experimental method is summarized in Sec. II. Section III contains the presentation of the results on the $6snf$ configurations and an analysis thereof. In Sec. IV this analysis is extended and subjected to critical evaluation. Finally Sec. V is devoted to the $6snp$ configuration.

II. EXPERIMENTAL METHOD

The experimental procedure differs in some aspects from that of our earlier publications on high-resolution spectroscopy.[6–8] High resolving power is obtained in a setup where the output beam of a narrow-band laser source orthogonally intersects an atomic beam of barium. Ultraviolet radiation is employed to excite barium atoms from metastable states to the levels just below the ionization limit. The uv radiation is produced by frequency doubling inside a frequency-stabilized cw ring dye laser (Spectra-Physics 380D) operating on Rhodamine-6G, using ammonium dihydrogen arsenate (ADA) as a nonlinear crystal.[7,8] In general a few mW is sufficient to efficiently populate the Rydberg states. The atomic beam of barium, emerging from a radiatively heated oven, is strongly collimated resulting in a residual Doppler width of a few MHz. A fraction of the atoms is transferred to metastable states by a discharge which runs through the oven nozzle.

The Rydberg state population is monitored using field ionization, a technique particularly suited in combination with a rarefied atomic beam. In earlier atomic beam experiments on Rydberg states a pulsed laser was used, enabling *in situ* detection of the excited atoms after the laser pulse had ended.[9] In the present experiment, where a cw light source is employed, the temporal delay between the excitation and the ionization of an atom is a result of a spatial separation between excitation and ionization region. Spatial separation of the order of a few mm is allowable as the decay rate of Rydberg states to low-lying levels is relatively low ($10^3 - 10^6$ s^{-1}) and thermal velocities are of the order of 500 m/s. The detector assembly is a block of solid copper in which holes have been drilled for the atomic beam and for the laser beam such that these channels are orthogonal. The excitation region is thus defined by the intersection of these channels. Three millimeters downstream from this intersection the atomic beam enters the gap of a parallel plate capacitor, which sets up the ionization field. The electrons are repelled by the negatively charged lower plate and escape through a mesh in the grounded upper plate of the capacitor. The electrons are captured on the cathode of an electron multiplier (Galileo CEM 4039) which delivers a short current pulse for each impinging charged particle. This detector is not state selective, i.e., it is not possible to probe the dynamics of population transfer between Rydberg levels, e.g., as a result of blackbody radiation. This is a consequence of the continuous nature of the experiment. Although the efficiency of the detector is not unity, due to partial decay to low-lying levels during the transit to the detector, it is still very high compared to any optical detection scheme, in particular for values of the principal quantum number $n \geq 20$.

The electron multiplier signal is processed by a photon counting system and stored on a minicom-

puter, together with the calibration signal of a confocal Fabry-Perot interferometer of ~150 MHz free spectral range. The interferometer is locked to an iodine-stabilized HeNe laser.

A fringe-counting wave meter, similar to the design of Hall and Lee is used to adjust the laser frequency close to the atomic transition frequency.[10] It is also employed for a careful measurement of this frequency to within 100 MHz. The iodine-stabilized HeNe laser is then used as a reference light source.

We have studied excitations starting from $5d\,6s\,{}^3D_1$ to $6snf$ ($n \geq 19$) and $6snp$ ($n \geq 21$) or from $5d\,6s\,{}^3D_2$ to $6snf$ ($n \geq 20$) and $6snp$ ($n \geq 22$). The lower limit on this number is imposed by the frequency-doubling crystal (ADA). At these values of n the phase matching temperature of the crystal closely approaches the reordering transition temperature. As no other crystal obeys 90° phase matching in the region between 307 and 316 nm no attempt has been made to probe the structure of the odd-parity states for lower n values. For the same reason transitions originating from both the $5d\,6s\,{}^1D_2$ and ${}^3D_3$ metastable states were not studied.

Strong signals are observed for the transitions leading to the $6snf$ states, whereas the signals in transitions to the $6snp$ configurations are orders of magnitude weaker, precluding in most cases the observation of the spectrum of the odd isotopes.

III. ANALYSIS

In Fig. 1 some examples are shown of excitation spectra $5d\,6s\,{}^3D_1 \rightarrow 6snf$. Essentially all spectral components are due to the odd isotopes ^{135}Ba and ^{137}Ba. The abundancy in a natural sample of these isotopes, both with nuclear spin $I = \frac{3}{2}$, equals 6.6% and 11.1%, respectively. In the spectra shown in Fig. 1 the even isotopes ($I = 0$) give rise to a closely spaced multiplet which, although merged into one peak in the examples given, can partly be separated in more detailed scans. This multiplet represents the

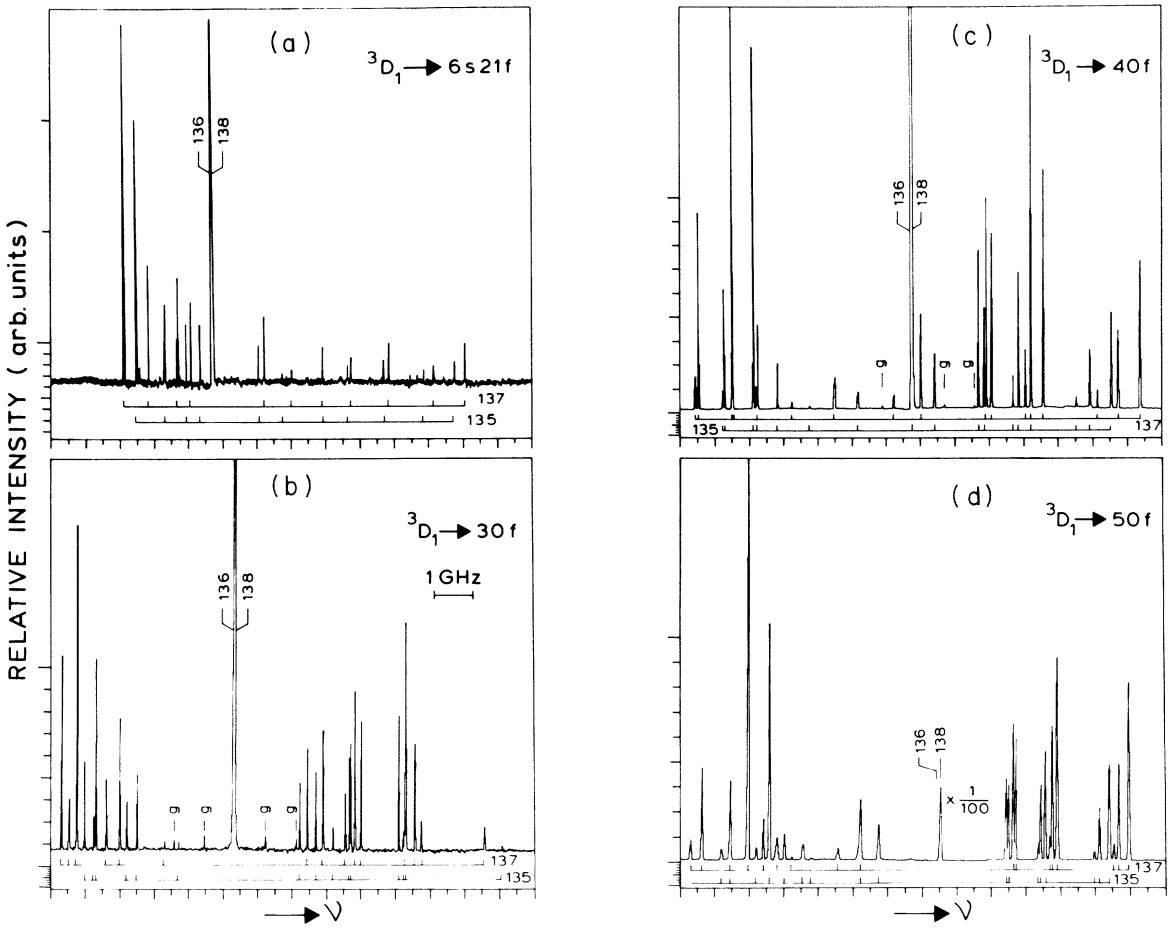

FIG. 1. Excitation spectra $5d\,6s\,{}^3D_1 \rightarrow 6snf$ for $n = 21$, 30, 40, and 50. The assignment to the various isotopes is indicated. g indicates a peak induced by a laser ghost.

transition $^3D_1 \rightarrow 6snf\,^3F_2$. For each of the odd isotopes ^{135}Ba and ^{137}Ba, 17 components are detected in most of the excitation spectra. The excitation $^3D_1 \rightarrow 6snf\,^3F_2$, however, has eight components only. This indicates that for the odd isotopes the electronic angular momentum quantum number J is no longer a good quantum number and that strong mixing of the fine-structure states induced by the hyperfine interaction is observed.

Following Barbier and Champeau we postulate that the energy splittings within a configuration $6snl$ are induced by the Hamiltonian

$$H_1 = \frac{1}{r_{12}} + \xi_{nl}\vec{s}\cdot\vec{l} + a_c\vec{s}\cdot\vec{I} \ , \tag{1}$$

where $1/r_{12}$ represents the Coulomb repulsion between the two valence electrons, $\xi_{nl}\vec{s}\cdot\vec{l}$ represents the effective spin-orbit interaction of the Rydberg electron and $a_c\vec{s}\cdot\vec{I}$ represents the effective Fermi contact hyperfine interaction of the $6s$ electron, which is nonzero only for the odd isotopes ($I \neq 0$). Other interactions, such as the hyperfine interaction of the Rydberg electron and spin-spin and spin—other-orbit interactions, are here assumed to be negligible. The radial wave functions of the two valence electrons which determine the values of the interaction strengths for all three terms in H_1, are eigenfunctions of a zero-order central field Hamiltonian, which also accounts for the shielding of the two valence electrons. These radial wave functions will not be considered here. To calculate the energy splittings within the configuration $6snl$ we choose the standard coupling scheme to construct the basis states

$$|\,6snlSLIJF\rangle \ ,$$

where S represents the total electronic spin ($S=0$ or $S=1$), L the total orbital angular momentum ($L=l$), I the nuclear spin, J the total electronic angular momentum ($\vec{J}=\vec{S}+\vec{L}$), and F the total angular momentum ($\vec{F}=\vec{J}+\vec{I}$).

The first-order energy contributions of H_1 are described by four parameters: $F^0(6s,nl)$, $G^l(6s,nl)$, ξ_{nl}, and a_c. The direct Slater integral $F^0(6s,nl)$ does not induce any splittings between the various sublevels of the $6snl$ configuration and cannot be determined. According to a hydrogenic model the parameters $G^l(6s,nl)$ and ξ_{nl} vary as $(n^*)^{-3}$ where n^* represents the effective principal quantum number. The Fermi contact parameter, however, is independent of n^*, as the hyperfine interaction is related to the nonexcited electron. Consequently, for the odd isotopes the hyperfine interaction will be the dominating term in H_1 for sufficiently large values of n and will induce severe fine-structure state mixing, which is indeed observed (see Fig. 1). In the limit $n \rightarrow \infty$ the structure of the excited state for these isotopes will collapse into a doublet, corresponding to the ground-state hyperfine doublet of Ba II, whereas for the even isotopes only one single component will persist. This correspondence leads to the equation ($I=\frac{3}{2}$)

$$a_c = A(\text{Ba II}, 6s\,^2S_{1/2}) \ , \tag{2}$$

where $A(\text{Ba II}, 6s\,^2S_{1/2})$ represents the magnetic dipole hyperfine coupling constant of the Ba II ground state, very well known from high-precision experiments.[11]

Owing to the presence of isotopes without nuclear spin it is in principle possible to analyze the n-dependent interactions quite simply. The relative positions of the $^3F_2$, $^3F_3$, and $^1F_3$ levels can be measured in excitations from the metastable $5d\,6d\,^3D_2$ level, sufficient to extract values for the two relevant interaction parameters $G^3(6s,nf)$ and ξ_{nf}. However, initially the component $^3D_2 \rightarrow {}^1F_3$ was not observed, preventing such a direct evaluation of $G^3(6s,nf)$ and ξ_{nf}. Only excitations from $^3D_3$ would provide the required data, but such spectra can not be taken with the available experimental setup. Consequently, the interaction parameters have to be extracted from the odd isotopes.

In the odd-isotope spectrum both the lower-state and excited-state hyperfine quantum numbers of almost all components can be assigned unambiguously with the aid of the known lower-state hyperfine splitting and the $\Delta F = 0, \pm 1$ selection rule.[12] The spectra of both odd isotopes are expected to be similar since the magnetic contribution to the hyperfine interaction dominates and the nuclear magnetic moment ratio is close to 1.[12] The intensity ratio of identical components then roughly equals the abundancy ratio (~ 1.7 for ^{137}Ba/^{135}Ba).

In order to extract the interaction parameters $G^3(6snf)$, ξ_{nf}, and a_c from the observed spectra the Hamiltonian of Eq. (1) is diagonalized in the $|\,SLJF\rangle$ basis within the configuration $6snf$. A spectrum is generated by taking along the lower-state hyperfine energies and calculating relative transition probabilities, resulting in a spectrum of 23 components per odd isotope for excitations starting from $^3D_1$ and of 34 components for excitations starting from $^3D_2$. Preceding a fit between the calculated and experimental spectra the ordering of the hyperfine transitions has to be identical. This ordering sensitively depends on the initial values of $G^3(6snf)$, ξ_{nf}, and a_c. The former parameters are assumed to be positive with $G^3(6snf) \gg \xi_{nf}$, reflecting the low transition strengths from $^3D_1$ to $^1F_3$. a_c is set equal to the hyperfine interaction constant of

the Ba II ground state for the relevant isotope [see Eq. (2)]. The observed strong mixing in, e.g., the $^3D_1 \rightarrow 6s\,45f$ excitation spectrum leads to the ordering

$$G^3(6s\,45f) > a_c > \xi_{45f} \ . \tag{3}$$

Following these considerations initial values for the aforementioned parameters are found which yield the correct ordering of the hyperfine transitions. Final values for the parameters can then be extracted by fitting the calculated energy spectrum to the experimental spectrum. We employ the MINUIT routine from the CERN (European Center for Nuclear Research) library for this procedure.[12] For the excitation $^3D_1 \rightarrow 6s\,45f$, a typical example, the rms difference between experimental and calculated energies amounts to $^{137}\langle \Delta\nu \rangle_{\rm rms} = 77$ MHz, the index referring to the odd isotope considered. Table I contains the results of the fit. $^{137}a_c$ is indeed within 0.1% of the ionic value [Eq. (2)], giving support to the analysis. In addition the relative transition strengths are quite well predicted, too. However, the rms difference is much larger than the experimental error (~ 1 MHz). Furthermore, the very weak transition to $^1F_3$, not included in the fit, were later found to lie at appreciably higher energy than predicted.

IV. FURTHER ANALYSIS AND DISCUSSION

Considering the discrepancies between calculated and observed spectra we conclude that diagonalizing the Hamiltonian of Eq. (1) within the configuration $6snf$ is inadequate. Consequently, the parametrization of the energies with the parameters $G^3(6snf)$, ξ_{nf}, and a_c has to be extended either by adding interactions which have been considered negligible so far or by including higher-order effects of the Hamiltonian of Eq. (1) in an effective way. Since the introduction of an additional parameter improves a fit in general it is necessary to choose between possible candidates *a priori* by making order of magnitude estimates.

A. Additional interactions

A number of additional interactions are considered: hyperfine interaction of the Rydberg electron, spin-spin interaction, and spin—other-orbit interaction.

(i) Hyperfine interaction of the Rydberg electron. The Rydberg electron has orbital angular momentum $l=3$ and thus, neglecting relativistic effects, can interact with the nucleus via the two types of dipole interactions $[\vec{l}\cdot\vec{I}$ and $(\vec{s}C^{(2)})^{(1)}\cdot\vec{I}$, representing the interaction of the nuclear magnetic dipole moment with the orbital motion of the electron and the dipole-dipole interaction between the spins of the nucleus and electron, respectively] or via the classical quadrupole interaction.[13] The strengths of these hyperfine interactions are measured by $\langle r^{-3} \rangle_{nf}$ which scales like

$$\langle r^{-3} \rangle_{nf} \sim (n^*)^{-3} \tag{4}$$

according to the hydrogenic model. $\langle r^{-3} \rangle_{45nf}$ can, e.g., be estimated by scaling a Hartree-Fock result[14]:

$$\langle r^{-3} \rangle_{7f} = 2 \times 10^{-4} a_0^{-3} \ .$$

This results in

$$a_{45f} \sim 45 \text{ Hz} \ ,$$

where a_{nl} represents the one-electron hyperfine parameter[13] (similar to a_c). The hyperfine splittings which are of the same order of magnitude are too small to improve the energy parametrization.

(ii) The spin-spin interaction and spin—other-orbit interaction. These two interactions and the spin—own-orbit interaction all scale as $\langle r^{-3} \rangle$; thus the relative interaction strengths are expected to be independent of n.[15,16] Different scaling laws apply as a function of the nuclear charge Z, i.e, Z^4 for the normal spin-orbit interaction and Z^3 for the two-body terms. On the basis of this scaling law and the known relative strengths in helium the strength of these two-body effects is estimated to be less than 1% of the strength of the one-body term.

An order-of-magnitude estimate for the spin-spin energy is obtained from a Hartree-Fock calculation of the spin-orbit parameter ξ_{nf} and the Marvin integral $M^0(6snf)$ which characterizes the spin-spin energies in a $6snl$ configuration[17]:

$$\xi_{7f} = 2 \times 10^{-2} \text{ cm}^{-1} \ ,$$

$$M(6s\,7f) = 4 \times 10^{-5} \text{ cm}^{-1} \ .$$

The ratio M^0/ξ is indeed small, indicating that the spin-spin interaction should not be added to the energy parametrization. The spin—other-orbit interaction which is on equal footing with the spin-spin interaction is also discarded.

B. Higher-order effects

So far the calculation of the perturbation energy has been done in first order only, i.e., it is limited to a single configuration $6snf$. However, the $6snf$ configurations can interact with configurations of identical parity such as other $6snf$ configurations and with levels of the $5dnp$ series. Interactions with members of the latter series are expected to be rather localized, and only for $n=20$ an indication of a lo-

calized perturbation is found. We will consider configuration interaction in more detail; reference is made to diagrammatic techniques.[18]

The three terms in the Hamiltonian H_1 are represented by the single diagrams of Fig. 2. The second-order energy of H_1 has six terms, representing all different combinations of the three diagrams. Three of these terms pertain to diagrams where the same operator occurs twice. With the aid of angular momentum graphical techniques it can be shown that for configurations *msnl* the *LS* dependence of these three diagrams occurring in second order is identical to the *LS* dependence of the respective first-order diagrams. Consequently, these second-order energies can be included in the first-order energies by modifying the interaction parameters [i.e., Slater parameters $F^0(msnl)$, $G^l(msnl)$, spin-orbit parameter ξ_{nl}, and Fermi contact parameter a_c]. This is valid for all orders of perturbation when higher-order diagrams of the same interaction are considered. The higher-order diagrams of the spin-orbit and hyperfine interactions, respectively, represent *one-body* effects, whereas any diagram containing the electrostatic repulsion represents *many-body* effects.

Of the three remaining second-order diagrams the combined hyperfine–spin-orbit diagram is zero. No such diagram can be constructed. The two remaining diagrams, representing combinations of the electrostatic repulsion and the hyperfine interaction or spin-orbit interaction represent effective *two-body* effects. Only the "exchange" two-body diagrams differ in *SL* dependence from the corresponding one-body diagrams and give rise to new effective parameters. These "exchange" two-body diagrams are shown in Fig. 3.

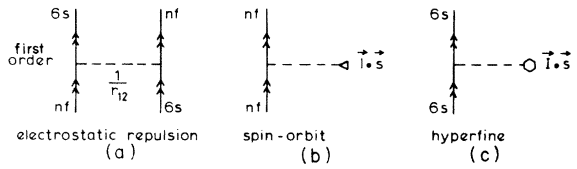

FIG. 2. Diagrams representing the three terms in Hamiltonian H_1 [Eq. (1)].

The intermediate states in Fig. 3 are of the type $6sn'f$ $(n'\neq n)$ for the effective two-body spin-orbit interaction (TBSO) and of the type $msnf$ $(m\neq 6)$ for the effective two-body hyperfine interaction (TBH), as follows directly from the conservation of angular momentum. The energy expressions corresponding to these two-body terms are

$$E(\mathrm{TBSO}) \sim \sum_{n'f} \frac{\langle 6snfS'LJ \mid r_{12}^{-1} \mid 6sn'fS'LJ\rangle \langle 6sn'fS'LJ \mid H_{\mathrm{so}} \mid 6snfSLJ\rangle}{\epsilon_{nf}-\epsilon_{n'f}}, \tag{5a}$$

$$E(\mathrm{TBH}) \sim \sum_{\substack{ms \\ m\neq 6}} \frac{\langle 6snfSLJ \mid r_{12}^{-1} \mid msnfS'LJ\rangle \langle msnfS'LJ \mid H_{\mathrm{hyp}} \mid 6snfSLJ\rangle}{\epsilon_{6s}-\epsilon_{ms}}, \tag{5b}$$

respectively. According to the hydrogenic model both E(TBSO) and E(TBH) scale as $(n^*)^{-3}$. The denominators in (5a) and (5b) differ by many orders of magnitude, since the energy separation between Rydberg configurations is very small compared to the separation between low-lying valence states, whereas the numerators are roughly of the same order of magnitude. Thus we expect that E(TBSO) is appreciably larger than E(TBH).

In conclusion it seems feasible to extend the parametrization of the energy splittings within the configuration $6snf$ with a term representing the effective two-body spin-orbit interaction. The less probable effective two-body hyperfine interaction will however not yet be discarded altogether.

C. Extended analysis

The relative energies within the configuration $6snf$ are, for a single odd isotope, summarized in four interaction parameters $G^3(6snf)$, ξ_{nf}, a_c, and $\alpha(6snf)$, where the latter represents the two-body effect. The energy matrix representing the *SLJF* dependence of the two-body term is obtained by a symmetrized matrix multiplication of the relevant first-order matrices (i.e., of the exchange electrostatic matrix and the spin-orbit matrix for the TBSO term). Energies are now calculated by a diagonalization of the Hamiltonian H_1 extended with the two-body term. Compared to the earlier analysis the fit to the observed spectra is appreciably improved with the inclusion of the two-body spin-orbit interaction:

$$^{137}\langle \Delta\nu\rangle_{\mathrm{rms}}^{\mathrm{TBSO}} = 6.3 \text{ MHz},$$

a decrease by a factor of 12. The effect of TBH on the rms frequency difference is less drastic:

$$^{137}\langle \Delta\nu\rangle_{\mathrm{rms}}^{\mathrm{TBH}} = 31 \text{ MHz}.$$

In view of these results and the order of magni-

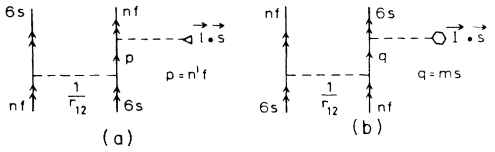

FIG. 3. Diagrams representing (a) the two-body spin-orbit interaction and (b) the two-body hyperfine interaction. The intermediate-state summation runs over all $6sn'f$ ($n' \neq n$) configurations (left) and $msnf$ ($m \neq 6$) configurations (right), respectively.

tudes as discussed in the previous section the effective two-body spin-orbit term is believed to be the most suitable addition to the energy parametrization. Further arguments sustaining this choice will be put forward in consecutive sections.

The four-parameter calculated spectrum $^3D_1 \rightarrow 6s\,45f$ is shown in the fifth column of Table I together with the earlier calculated three-parameter spectrum which forms the third column. Indeed, the frequency differences, i.e., $\nu_{\text{calc}} - \nu_{\text{expt}}$ (the sixth and fourth columns, respectively) have decreased drastically. Major differences are observed in the calculated positions of the so far unobserved weak components. The values of the parameters $G^3(6snf)$ and ξ_{nf} are seen to be rather drastically affected by the introduction of the parameter α, whereas a_c is unchanged, as is tc be expected.

The remaining frequency differences are difficult to assess. They are in general too small ($\lesssim 5$ MHz) to warrant the introduction of an additional energy parameter. For some hyperfine levels the differences are larger. This deviation appears systematically in the observed spectra. We have attempted to attribute these remaining deviations also to the use of a too simple model. The quality of the fit is not improved significantly by adding the TBH term, considered as a reasonable candidate, to the extended energy expression.

Neglecting energy contributions arising in higher order of perturbation theory we conclude that the energy splittings within a $6snf$ configuration are sufficiently well described with the four-parameter energy expression.

TABLE I. Experimental and calculated spectrum $5d\,6s\,^3D_1 \rightarrow 6s\,45f$ using a three-parameter and a four-parameter model. The relative intensities, tabulated in the last column are a result of the four-parameter calculation. All frequency values in MHz.

	$\xi_{45f}=710$ MHz $G^3(6s\,45f)=19\,560$ MHz $a_c=4021.3$ MHz			$\xi_{45f}=858.7$ MHz $G^3(6s\,45f)=31\,984.5$ MHz $a_c=4014.1$ MHz $\alpha(6s\,45f)=1932.2$ MHz		
$F_{\text{gro}}\ F_{\text{exc}}$	Expt.	Calculated	Difference	Calculated	Difference	Intensity
2.5→1.5		+5434.58		+8796.46		0.0002
2.5→2.5		+5237.55		+8490.73		0.0038
2.5→3.5		+4928.60		+8024.11		0.0207
1.5→1.5		+4146.48		+7608.36		0.0025
1.5→2.5		+3949.45		+7202.63		0.0110
0.5→1.5		+3319.56		+6681.44		0.0031
2.5→3.5	−418.20	−246.85	+171.35	−413.75	+4.45	0.2088
2.5→2.5	−713.80	−646.24	+67.56	−708.28	+5.52	0.1063
2.5→1.5	−869.40	−901.81	−32.41	−870.52	−1.12	0.0178
1.5→2.5	−1999.90	−1934.34	+65.56	−1996.38	+3.52	0.3043
1.5→1.5	−2158.80	−2189.81	−31.11	−2158.62	+0.18	0.2337
1.5→0.5	−2234.90	−2333.01	−98.11	−2239.82	−4.92	0.0450
0.5→1.5	−2983.90	−3016.83	−32.93	−2985.54	−1.64	0.2840
0.5→0.5	−3060.40	−3159.93	−99.53	−3066.74	−6.34	0.3500
2.5→3.5	−5600.00	−5739.01	−139.01	−5583.50	+16.50	0.0768
2.5→2.5	−6166.00	−6130.85	+35.15	−6167.08	−10.08	0.0136
1.5→2.5	−7454.00	−7418.95	+35.05	−7464.18	−10.18	0.0390
2.5→1.5	−7609.20	−7636.83	−27.63	−7609.21	−0.01	0.0040
2.5→2.5	−8276.50	−8207.00	+69.50	−8237.31	+3.19	0.0743
2.5→3.5	−8698.00	−8689.28	+8.72	−8693.81	+4.19	0.5736
1.5→1.5	−8896.00	−8924.93	−28.93	−8897.31	−1.31	0.0518
1.5→2.5	−9561.00	−9495.10	+65.90	−9561.41	−0.41	0.2127
0.5→1.5	−9722.70	−9751.85	−29.15	−9724.23	−1.53	0.0630

We have tried to use some of the rejected alternative additional energy distributions as a substitution of the TBSO term. All three terms which were tested, the spin-dipole hyperfine interaction, the orbital hyperfine interaction, and the spin-spin interaction do not yield satisfying fits, indicating that the selection of TBSO is not only justified on the basis of the order of magnitude estimates but also on the basis of the spin-angular dependence.

D. Results

The level structure for a single odd isotope has been analyzed in all configurations studied to yield the four interaction parameters $G^3(6snf)$, ξ_{nf}, $\alpha(6snf)$, and a_c representing the effective values for the Slater exchange, one-body spin-orbit, two-body spin-orbit, and Fermi contact hyperfine parameter, respectively. Additionally a fifth parameter is obtained $[(\Delta\nu)_{ca}]$ which relates to the shift of the spectrum relative to the configuration average. This last parameter can, in principle, be used to obtain isotopic shift values.

The four interaction parameters are given in Table II as a function of n. The major part of these data has been extracted from $^3D_1 \rightarrow 6snf$ excitations. An exception is the $n=25$ result ($^3D_2 \rightarrow 6s\,25f$), marked by an asterisk. The results for the configuration $6s\,20f$ are not shown, although the level structure has been measured carefully. This level turns out to be perturbed appreciably.

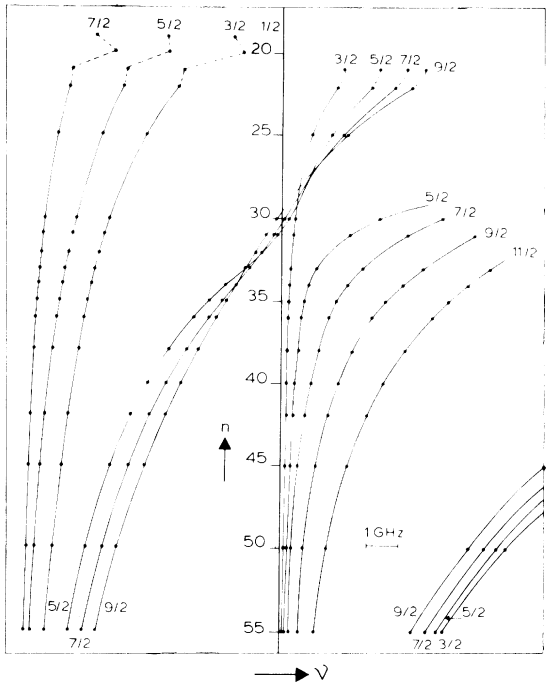

FIG. 4. Experimental hyperfine-level diagram of the $6snf$ configurations for various n. The $^3F_2$, $F=\frac{1}{2}$ hyperfine level is used as a reference level ($\nu=0$). Hyperfine quantum numbers are indicated. The solid and dashed lines serve to guide the eye only.

Insight into the effect of the hyperfine interaction can be gained from a diagram as shown in Fig. 4,

TABLE II. Interaction parameters $G^3(6snf)$, ξ_{nf}, $\alpha(6snf)$, $^{137}a_c$ and $^{135}a_c$ extracted from our spectra $5d\,6s\,^3D_1 \rightarrow 6snf$. The $n=25$ result denoted by an asterisk, results from an analysis of the $5d\,6s\,^3D_2 \rightarrow 6s\,25f$ excitation spectrum. All values in GHz.

n	$G^3(6snf)$	ξ_{nf}	$\alpha(6snf)$	$^{137}a_c$	$^{135}a_c$
19	1269	36.0	97.1	3.999	3.575
21	943	30.2	95.3	3.994	3.567
22	782	24.3	76.0	4.008	3.583
25*	392(1)	11.3(1)	24.1	4.018(4)	3.593
30	159.2(2.0)	4.39(2)	12.1(2)	4.105(4)	3.589
31	140.6(2.0)	3.82(2)	10.5(2)	4.013(4)	3.589
32	123.1(2.0)	3.33(3)	8.93(18)	4.013(3)	3.585
33	105.2(2.8)	2.89(4)	7.55(20)	4.014(3)	3.586(3)
34	93.0(3.0)	2.54(3)	6.55(20)	4.019(4)	
35	80.7(3.0)	2.20(4)	5.42(25)	4.023(3)	
36	72.8(2.0)	2.01(2)	4.98(15)	4.011(3)	3.586(3)
38	59.6(1.0)	1.623(10)	3.97(10)	4.014(3)	3.588(5)
40	46.1(1.8)	1.311(20)	3.05(18)	4.009(8)	3.588(6)
42	41.1(7)	1.105(8)	2.61(8)	4.015(3)	3.588(3)
45	32.0(4)	0.849(7)	1.92(3)	4.014(3)	3.586(3)
50	22.8(5)	0.601(6)	1.36(3)	4.013(3)	3.586(7)
55	16.9(5)	0.427(8)	0.98(10)	4.011(8)	3.585(8)

where part of the hyperfine level structure as derived from the observed spectra is displayed as a function of n (vertical axis). In the figure the single $F=\frac{1}{2}$ hyperfine level, occurring only in $^3F_2$, serves as a reference level and the points corresponding to this level fall on this vertical axis. A region of about 16 GHz total width is shown around the $F=\frac{1}{2}$ level. This region is selected since most of the transition strength in $^3D_1 \rightarrow 6snf$ or $^3D_2 \rightarrow 6snf$ excitations lies in this interval. At the bottom of the figure (high-n side) an onset of convergence of the hyperfine level structure into a hyperfine doublet (that of the Ba II $6s\ ^2S_{1/2}$ ground state) is visible. The levels on the high-energy side (right-hand side in the figure) converge to the Ba II ground-state hyperfine level $F=2$, whereas the remaining six levels converge to the Ba II $F=1$ hyperfine level. A triplet of levels, $F=\frac{5}{2}$, $\frac{7}{2}$, and $\frac{9}{2}$, starting in the lower left section of Fig. 4 cross each other repeatedly in the interval $n=22-35$ due to anticrossing with nearby levels of the same signature. The crossings in this region are quite sensitive to the parameters $G^3(6snf)$, ξ_{nf}, and $\alpha(6s,nf)$ and thus measure these parameters rather accurately.

Thus far only the hyperfine quantum number has been assigned, as the total spin S and the electronic angular momentum J are not conserved. It is however possible to assign to each hyperfine level asymptotic values for S and J. At $n=22$ a clear grouping has developed, which enables such an assignment. The quartet of levels appearing in the lower right corner of Fig. 4 has $^1F_3$ character (see next subsection). The group of levels $F=\frac{5}{2}-\frac{11}{2}$ which bend off at the right-hand side belong to "$^3F_4$." At the top of the figure the four levels at the right of $F=\frac{1}{2}$ are predominantly "$^3F_3$" while the remaining four levels are to be assigned "$^3F_2$." This assignment is corroborated by calculating the projections of the energy eigenstates on the basis states $|SLJF\rangle$. As an example we show in Fig. 5 the squared coefficients in the expansion of the four $F=\frac{5}{2}$ eigenstates on the $|SLJ\rangle$ basis states $|\,^1F_3\rangle$, $|\,^3F_4\rangle$, $|\,^3F_3\rangle$, and $|\,^3F_2\rangle$. The graphs are ordered according to increasing energy, i.e., from left to right in Fig. 3. They show clearly the expected increase of fine-structure state mixing with increasing n. The anticrossing near $n=32$ comes out particularly clearly as an exchange of $J=4$ character between the eigenstates corresponding to graphs (b) and (c). The graphs are also of aid in understanding the trend in the intensity distribution as a function of n. In transitions starting from $^3D_1$ the relative strengths of the components leading to the four $F=\frac{5}{2}$ hyperfine levels reflect directly the "$^3F_3$" components in the eigenstates.

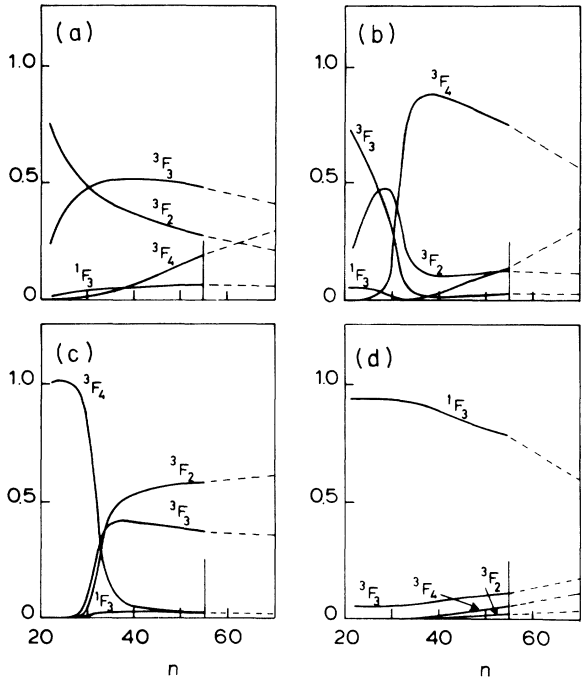

FIG. 5. The composition of the four $F=\frac{5}{2}$ eigenstates as a function of n ordered according to increasing energy (see Fig. 4),

$$|F=\tfrac{5}{2}\rangle=\alpha\,|\,^1F_3,\tfrac{5}{2}\rangle+\beta\,|\,^3F_4,\tfrac{5}{2}\rangle+\gamma\,|\,^3F_3,\tfrac{5}{2}\rangle+\delta\,|\,^3F_2,\tfrac{5}{2}\rangle\ .$$

α^2, β^2, γ^2, and δ^2 are shown. The dashed parts of the curves represent the extrapolation to infinite n. The vertical bars indicate the limit of the experiment.

E. Internal consistency checks

In this section we will discuss the consistency of our analysis when further data are taken into account. According to our model the hyperfine interaction parameter a_c obeys Eq. (2) and thus is independent of n. The experimental values for a_c, collected in Table II are indeed constant for $n \geq 25$. Average values for the hyperfine parameters for ^{135}Ba and ^{137}Ba, taken for the interval $n=15-55$, are given in Table III together with the magnetic dipole hyperfine interaction constants of the Ba II ground states.[11,19] The agreement is good. The experimental results for $n<25$ are excluded as the experimental information becomes increasingly scarce for low n due to a decrease in fine-structure state mixing (see Fig. 5).

Second, the isotope independent parameters, $G^3(6snf)$, ξ_{nf}, and $\alpha(6snf)$ can be extracted from

TABLE III. The Fermi contact parameters extracted from the Rydberg spectra. In addition the hyperfine-interaction constants of Ba II, $6s\ ^2S_{1/2}$ are given.

$^{137}\bar{a}_c$	^{137}A(Ba II, $6s\ ^2S_{1/2}$)	$^{135}\bar{a}_c$	^{135}A(Ba II, $6s\ ^2S_{1/2}$)
4014.5(3.0)	4018.870 833 8(2)[a]	3587.7(2.2)	3593.4(3.0)[b]

[a]From Ref. 11.
[b]From Ref. 19.

the spectra of both odd isotopes. In addition we have measured excitations starting from both $5d6s\ ^3D_1$ and from $5d6s\ ^3D_2$ for a number of values of the principal quantum number n, resulting in up to four independent measurements of the parameters. Within the error ($\sim 1\%$) all values are in agreement. More details can be found elsewhere.[20]

Of most valuable aid in assessing the correctness of the energy parametrization are the components of the $^3D_1 \rightarrow 6snf$ "$^1F_3$" transition, very weakly allowed due to hyperfine-induced mixing of the $^1F_3$ and $^3F_2$ fine-structure states. A specimen of the spectrum corresponding to the transition to $6s40f\ ^1F_3$ is shown in Fig. 6. The integration time is increased by a factor of 20 with respect to the spectra displayed in Fig. 1; yet, not all components (six per odd isotope) can be found. Analogous spectra have been observed for $n = 45$, 50, and 55. The $^1F_3$ excitation spectra were actually measured only after the analysis had been completed and their positions and relative strengths had been predicted. The actual positions of the hyperfine components relative to the selected "^3F" components are in good agreement with the prediction of our four-parameter energy expression. These predicted frequencies are included in Table I. The calculated relative intensities in the last column of this table explain why these components were not observed in the earlier experiments and are only found in a dedicated search.

All other parametrizations of the energy, where one of the rejected alternatives for the effective two-body spin-orbit term is used instead do not predict the positions of the hyperfine sublevels of $^1F_3$ correctly. The deviations between experiment and prediction are then of the order of a few GHz.

A rather unexpected result of the present analysis is the behavior of the parameters $G^3(6snf)$, ξ_{nf}, and $\alpha(6snf)$ as a function of n, displayed in a double-logarithmic plot in Fig. 7, where two lines,

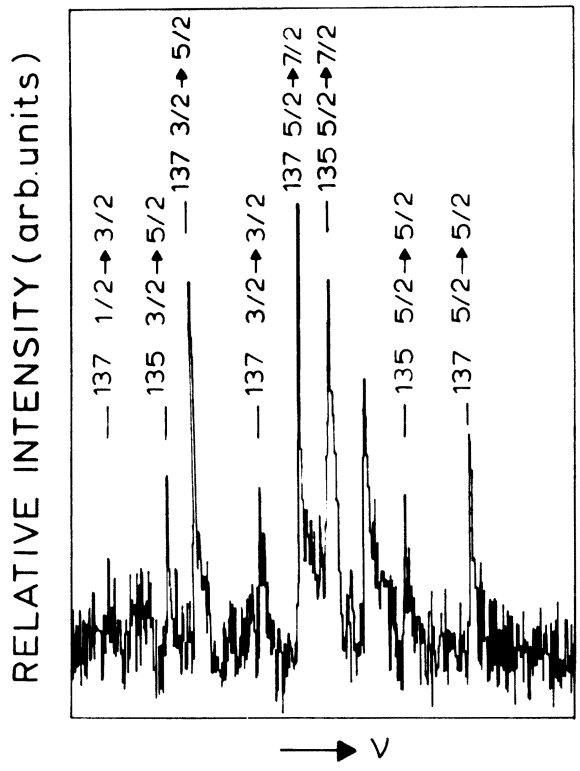

FIG. 6. Excitation spectrum $5d6s\ ^3D_1 \rightarrow 6s40f\ ^1F_3$. Hyperfine quantum numbers and isotopic assignments are given.

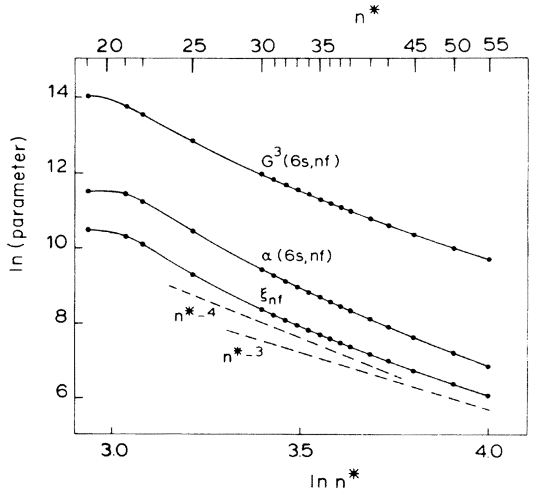

FIG. 7. Double-logarithmic plot of the n-dependent interaction parameters as a function of n^*. $(n^*)^{-3}$ and $(n^*)^{-4}$ dependences are indicated.

representing an $(n^*)^{-3}$ and an $(n^*)^{-4}$ dependence, are shown as well. Although the experimental data tend to behave according to the $(n^*)^{-3}$ law for the highest values of n, this is certainly not true around $n=30$. The curvature of the smooth line, which only serves to connect the data points, changes rather abruptly at $n=22$, due the presence of a nearby perturber state. The effect of this perturber comes out more clearly in Fig. 4.

The nonhydrogenic behavior, represented by the curvature in Fig. 7 is hitherto unexplained. The ratio of the parameters $G^3(6snf)/\xi_{nf}$ is approximately constant (~ 36) whereas the ratio $\alpha(6snf)/\xi_{nf}$ has a slight n dependence and ranges from 2.76 to 2.26 in the interval $n=30$ to $n=55$. These ratios are well suited for a comparison with *ab initio* calculations. Such calculations, however, have not yet been made.

The data of Table II allow us to calculate the fine-structure splittings (e.g., $^3F_3$-$^3F_2$) which can be compared with experimental results on the even isotopes. As a consequence of the earlier-mentioned experimental limitations results on only the $^3F_3$-$^3F_2$ fine-structure interval are available. The experimental and calculated values are compared in Table IV showing excellent agreement for the $^3F_3$-$^3F_2$ interval. The single results for the $^1F_3$-$^3F_3$ splitting for $n=45$ cannot be reproduced as well. The result of Gallagher *et al.*[21] for the $^1F_3$-$^3F_2$ interval for $n=24$, is orders of magnitude off, possibly due to an erroneous assignment.

The experimental and calculated values for the $^3F_3$-$^3F_2$ interval are gathered in a double-logarithmic plot in Fig. 8. A straight line yields a good fit with the individual calculated points in the interval $n=21$–45 where experimental values have been obtained. The individual points scatter slightly around the straight line. The slope equals $-3.14(5)$. The power-law dependence of the fine-structure splitting is surprising in view of the n dependence of the interaction parameters (see Fig. 7). The calculated $^3F_4$-$^3F_3$ interval, however, again does not obey a power law of n^* but has roughly the same n dependence as the interaction parameters. The behavior of the $^3F_3$-$^3F_2$ fine-structure interval is probably fortuitous.

TABLE IV. Experimental and calculated values for some fine-structure multiplet splittings. All values in MHz.

n	Experimental	Calculated
	$^3F_3$-$^3F_2$	
21	5384(2)	5383
25	3283(2)	3273
30	1725(2)	1717
32	1390(2)	1344
34	1137(3)	1148
36	942(2)	962
38	790(2)	797
40	668(2)	681
45	455(2)	483
	$^1F_3$-$^3F_3$	
45	9486(5)	10289
	$^1F_3$-$^3F_2$	
24	7980(300)[a]	144700

[a]From Ref. 21

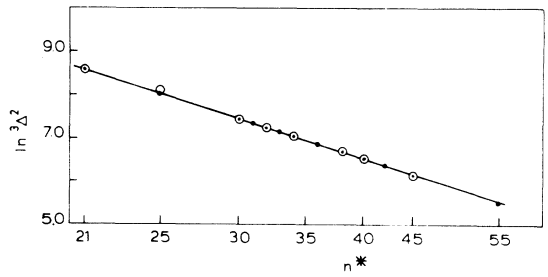

FIG. 8. Double-logarithmic plot of the fine-structure interval $^3F_3$-$^3F_2$ as a function of n^*.

F. The perturbation at $n=20$

In connection with irregularities in Figs. 4 and 7 we have noted the influence of a perturber around $n=20$. The intervals between the observed hyperfine components are perturbed to such an extent that the parameters $G^3(6snf)$, ξ_{nf}, $\alpha(6snf)$, and a_c cannot be extracted. The perturbation however is rather weak since it affects only a very limited range of n. Already the $n=19$ and 21 configuration can be analyzed with our energy parametrization, yielding parameter values reasonably in accord with values extrapolated from higher n. The presence of a perturbation with $J=2$ character, in this energy region, was observed earlier by Armstrong *et al.*[3] They observed a number of $6snf$ states $^3F_2$ ($n=17$–25) in an absorption spectrum from $6s\,7s\ ^3S_1$ indicating interaction between the $6snp$ and $6snf$ Rydberg series. The intensity distribution of the $^3S_1 \rightarrow {}^3F_2$ excitation shows a strong variation suggesting that the series interaction is restricted to the above-mentioned n interval. Energy level measurements indicate that the $6s\,20f\ ^3F_2$ state is shifted to lower energy.[3] The perturber is tentatively labeled $5d\,8p\ ^3P_2$.

G. Isotope shifts

The measurement of isotope shifts in transitions from low-lying valence states to Rydberg states en-

ables the determination of the level isotope shift of the lower level, as suggested by Niemax and Pendrill.[22] In combination with other transition isotope shift measurements level isotope shifts in a large set of levels can be determined[23,24] which can be compared with *ab initio* calculations.[25]

The isotope shift between the two most abundant even isotopes ^{138}Ba and ^{136}Ba is easily extracted from the experimental spectrum. The next-most-abundant even isotope ^{134}Ba is hidden under the ^{136}Ba isotope and the rare Ba isotopes ^{132}Ba and ^{130}Ba are not observed.

Isotope shifts between the odd isotopes can be evaluated from the $(\Delta\nu)_{ca}$ parameters for these isotopes (see Sec. IV D), representing the shift of the spectrum away from the average energy of the configuration. However, the errors in the $(\Delta\nu)_{ca}$ parameters are of the same order of magnitude as the difference $^{137}(\Delta\nu)_{ca}$-$^{135}(\Delta\nu)_{ca}$, precluding a determination of the even-odd isotope shifts, which require additional calculations, as well. Consequently, results are available only for the ^{136}Ba-^{138}Ba isotope shifts.

The residual level isotope shift of the $5d6s\ ^3D_J$ fine-structure states is obtained after subtracting the normal mass shift from the transition isotope shift and equals $^{136,138}\delta\nu_{res} = -16.1(5)$ MHz. No J dependence of the isotope shift is found.

V. THE 6*snp* CONFIGURATIONS

The 6*snp* configurations cannot be analyzed in detail as the signal strength in the recorded spectra is too low to identify a sufficient number of hyperfine components. For most values of the principal quantum number n only the even isotopes are observed. Nevertheless our measurements have yielded some new results.

Among the excitations $5d6s\ ^3D_1 \rightarrow 6snp$ the components leading to the $^1P_1$ levels are appreciably stronger than the components leading to $^3P_1$, even though the term mixing is expected to be small.[3]

Furthermore the excitations to $^1P_1$ have narrow linewidth (a few MHz full width at half maximum) up to very high values of n ($n \sim 80$), whereas the ^3P excitations broaden already at $n \sim 35$ and as a result become undetectable at $n \sim 40$.

Third, it has been found that careful term energy measurements are required to deduce a value for the ionization energy. An analysis of preliminary measurements on the $6snp\ ^1P_1$ levels indicate that the ionization energy equals $I_s = 42\,034.95 \pm 0.02$ cm^{-1} in excellent agreement with Armstrong's value.[3] The requirement that a unique value for the ionization energy exists leads to the conclusion that the 6*snf* configurations, which are hitherto believed to be unperturbed above $n = 22$, are possibly affected by an unidentified perturber. This conclusion is reached when it is tried to analyze the term energy values of the 6*snp* and 6*snf* configurations simultaneously.

VI. CONCLUSION

The present study of the odd-parity Rydberg states of barium has resulted in very detailed information on the structure of the 6*snf* configurations. The fine and hyperfine structure in these configurations have been analyzed simultaneously to yield quantitative information on two-body effects in the fine structure. The analysis of the hyperfine structure with an energy expression including these two-body effects shows a high level of internal consistency. In order to further support this analysis more experimental data have to be gathered with special emphasis on excitations of the type $5d6s\ ^3D_2 \rightarrow 6snf$ and $5d6s\ ^3D_3 \rightarrow 6snf$, in order to measure the fine-structure intervals $^3F_4$-$^3F_3$ and $^1F_3$-$^3F_3$. When all fine-structure intervals are known it will be possible to critically test the energy parametrization. An effort to study these excitations is currently being made in our laboratory.

Furthermore the incomplete results on the 6*snp* configuration require further study. In analogy with recent results on the 6*snd* configurations it is expected that such measurements can yield relevant information on fine-structure mixing and configuration interaction, enabling a critical test of multichannel quantum defect analyses.[3,26] Such a study is pursued as well.

Finally, interesting broadening phenomena have been observed for $n \geq 60$ resulting in, e.g., asymmetrical line shapes. A detailed study of these phenomena seems worthwhile.

ACKNOWLEDGMENTS

We are deeply indebted to J. Bouma, D. Breederveld, and B. H. Post for their assistance during the experiments and to Professor I. Lindgren for helpful comments. We gratefully acknowledge the Stichting voor Fundamenteel Onderzoek der Materie for financial support.

*Present address: Lyman Laboratory of Physics, Harvard University, Cambridge MA 02138.

[1]L. Barbier and R.-J. Champeau, J. Phys. (Paris) 41, 947 (1980).

[2]W. R. S. Garton and F. S. Tomkins, Astrophys. J. 158, 1219 (1969).

[3]J. A. Armstrong, P. E. Esherick, and J. J. Wynne, J. Opt. Soc. Am. 69, 211 (1979).

[4]J. L. Carlsten, T. J. McIlrath, and W. H. Parkinson, J. Phys. B 8, 38 (1975).

[5]P. Camus, R.-J. Champeau, S. Feneuille, S. Libermann, C. Morillon, and J. Pinard, Colloq. Int. C.N.R.S. 273, 67 (1977).

[6]E. R. Eliel, K. A. H. van Leeuwen, and W. Hogervorst, Phys. Rev. A 22, 1491 (1980).

[7]E. R. Eliel, W. Hogervorst, K. A. H. van Leeuwen, and B. H. Post, Opt. Commun. 36, 366 (1981).

[8]E. R. Eliel, W. Hogervorst, K. A. H. van Leeuwen, and B. H. Post, Opt. Commun. 39, 41 (1981).

[9]S. Libermann and J. Pinard, Phys. Rev. A 20, 507 (1979).

[10]J. L. Hall and S. A. Lee, Appl. Phys. Lett. 29, 367 (1976).

[11]R. Blatt and F. Worth, Phys. Rev. A 25, 1476 (1982).

[12]M. Gustavsson, G. Olsson, and A. Rosén, Z. Phys. A 209, 231 (1979).

[13]I. Lindgren and A. Rosén, Case Stud. At. Phys. 4, 150 (1974).

[14]J. Hansen, private communication.

[15]K.-N. Huang and A. F. Staroce, Phys. Rev. A 18, 354 (1978).

[16]H. Horie, Prog. Theor. Phys. 10, 296 (1953).

[17]H. H. Marvin, Phys. Rev. 71, 102 (1947).

[18]I. Lindgren and J. Morrison, *Atomic Many-Body Theory,* Springer Series in Chemical Physics 13 (Springer, Berlin, 1982).

[19]W. Becker, W. Fischer, and H. Hühnermann, Z. Phys. A 216, 142 (1968).

[20]E. R. Eliel, thesis Vrije Universiteit, Amsterdam, 1982 (unpublished).

[21]T. F. Gallagher, W. Sandner, and K. A. Safinya, Phys. Rev. A 23, 2969 (1981).

[22]K. Niemax and L. R. Pendrill, J. Phys. B 13, L461 (1980).

[23]C.-J. Lorenzen, K. Niemax, and L. R. Pendrill (unpublished).

[24]E. R. Eliel, W. Hogervorst, T. Olsson, and L. R. Pendrill (unpublished).

[25]A.-M. Mårtensson and S. Salomonsson, J. Phys. B 15, 2115 (1982).

[26]E. R. Eliel and W. Hogervorst (unpublished).